ACS central science

Research Article

Cite This: ACS Cent. Sci. 2018, 4, 260−267

An Aqueous Inorganic Polymer Binder for High Performance Lithium−Sulfur Batteries with Flame-Retardant Properties

Guangmin Zhou,[†,‡] Kai Liu,[†,‡] Yanchen Fan,[‡,§] Mengqi Yuan,[∥] Bofei Liu,[†] Wei Liu,[†] Feifei Shi,[†] Yayuan Liu,[†] Wei Chen,[†] Jeffrey Lopez,[⊥] Denys Zhuo,[†] Jie Zhao,[†] Yuchi Tsao,[†] Xuanyi Huang,[†] Qianfan Zhang,[*,§] and Yi Cui[*,†,#]

[†]Department of Materials Science and Engineering, Stanford University, Stanford, California 94305, United States

[§]School of Materials Science and Engineering, Beijing University of Aeronautics and Astronautics, Beijing, 100191, P. R. China

[∥]State Key Laboratory of Explosion Science and Technology, Beijing Institute of Technology, Beijing, 100081, P. R. China

[⊥]Department of Chemical Engineering, Stanford University, Stanford, California 94305, United States

[#]Stanford Institute for Materials and Energy Sciences, SLAC National Accelerator Laboratory, 2575 Sand Hill Road, Menlo Park, California 94025, United States

Supporting Information

ABSTRACT: Lithium−sulfur (Li−S) batteries are regarded as promising next-generation high energy density storage devices for both portable electronics and electric vehicles due to their high energy density, low cost, and environmental friendliness. However, there remain some issues yet to be fully addressed with the main challenges stemming from the ionically insulating nature of sulfur and the dissolution of polysulfides in electrolyte with subsequent parasitic reactions leading to low sulfur utilization and poor cycle life. The high flammability of sulfur is another serious safety concern which has hindered its further application. Herein, an aqueous inorganic polymer, ammonium polyphosphate (APP), has been developed as a novel multifunctional binder to address the above issues. The strong binding affinity of the main chain of APP with lithium polysulfides blocks diffusion of polysulfide anions and inhibits their shuttling effect. The coupling of APP with Li ion facilitates ion transfer and promotes the kinetics of the cathode reaction. Moreover, APP can serve as a flame retardant, thus significantly reducing the flammability of the sulfur cathode. In addition, the aqueous characteristic of the binder avoids the use of toxic organic solvents, thus significantly improving safety. As a result, a high rate capacity of 520 mAh g^{-1} at 4 C and excellent cycling stability of ∼0.038% capacity decay per cycle at 0.5 C for 400 cycles are achieved based on this binder. This work offers a feasible and effective strategy for employing APP as an efficient multifunctional binder toward building next-generation high energy density Li−S batteries.

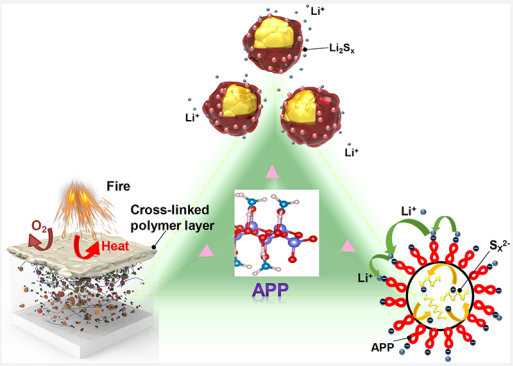

INTRODUCTION

As traditional intercalation transition metal oxide and phosphate cathode materials approach their theoretical capacity in lithium ion batteries (LIBs), it becomes challenging for them to meet the growing requirements for applications such as long-distance driving of electric vehicles.[1−3] Lithium−sulfur (Li−S) battery, one of the most promising next-generation high energy battery systems, has attracted significant attention due to its high theoretical specific energy, which is five times higher than that of state-of-art LIBs.[4,5] Meanwhile, sulfur is one of the most abundant elements on earth and is a byproduct of fossil fuel refining and gas desulfurization processes, making it available at low cost and at large scale.[6] Despite showing great promise, there are several problems which have impeded the practical application of Li−S batteries including the insulating nature of sulfur and Li_2S, safety issues caused by its high flammability, and serious side effects caused by soluble lithium polysulfides (LiPSs) and large volume change during charge/discharge processes.[7−9]

In the past decade, intense research efforts have focused on controlling polysulfides by physical confinement of sulfur within the pores of various carbon materials[10−16] or chemical immobilization of sulfur species through the introduction of polar hosts such as heteroatom doped carbon materials,[17,18] metal oxides,[19,20] metal sulfides,[21,22] and metal organic frameworks.[23] Significant effort has also been applied toward the development of coatings of organic polymers with LiPS trapping capability. For example, polyacrylonitrile−sulfur composites[24,25] or polyaniline nanotube or polyvinylpyrrolidone encapsulated sulfur cathodes[26,27] have been developed to reduce the dissolution and shuttle effect of polysulfides. Modification of separators or the introduction of an interlayer

Received: November 29, 2017
Published: February 14, 2018

DOI: 10.1021/acscentsci.7b00569
ACS Cent. Sci. 2018, 4, 260−267

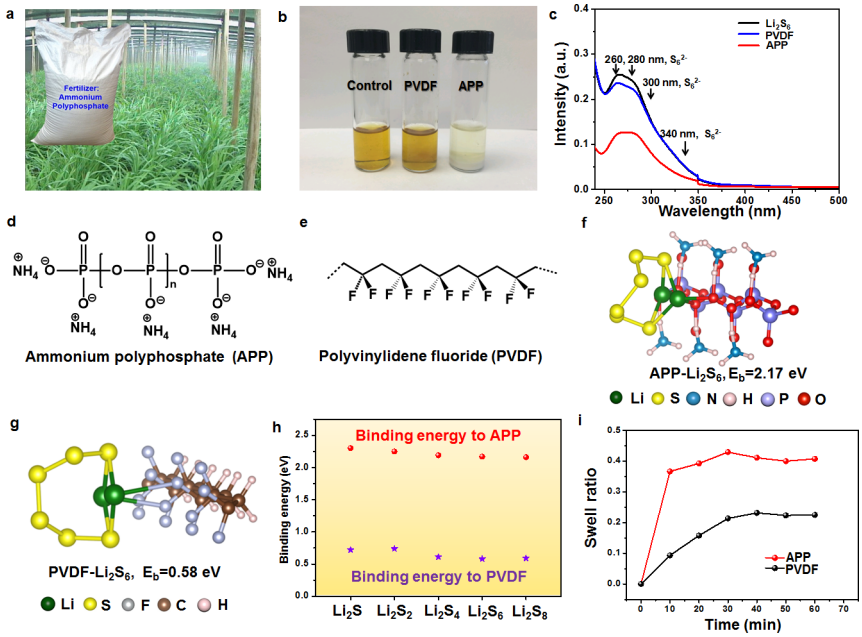

Figure 1. LiPS adsorption and swelling properties. (a) Commercially available APP used as fertilizer. (b) Digital image of the Li_2S_6 (0.005 M) captured by PVDF and APP in DOL/DME solution. (c) UV/vis absorption spectra of Li_2S_6 solution before and after the addition of PVDF and APP. Chemical structures of (d) APP and (e) PVDF binders. Adsorption conformations and binding strengths for Li_2S_6 on (f) APP and (g) PVDF polymers. (h) Binding strengths for APP and PVDF with various Li−S species. (i) Swelling ratios of the APP and PVDF binders.

is another promising route to trap polysulfides and reduce parasitic reactions.[28,29]

Another important approach to control polysulfides is through the polymer binder. Binders play a critical role in maintaining electrode integrity and ensuring sufficient contact between the cathode material and current collector during battery cycling. Polyvinylidene fluoride (PVDF) is the most commonly used binder for electrode preparation in Li−S batteries, requiring hazardous and expensive organic solvents such as *N*-methyl-2-pyrrolidone (NMP) to dissolve the PVDF as well as high temperature to dry the electrodes.[30] Instead, the use of aqueous binders as part of a green fabrication process is promising for Li−S battery application. In addition, aqueous binders are environmentally friendly and have the advantages of improved safety and low cost.[31] Therefore, aqueous binders such as gelatin,[32] carbonyl-β-cyclodextrin,[33] and poly(vinylpyrrolidone) (PVP)[34] have been tested in Li−S batteries.

Thus far, the polymer binders have always been organic in nature. Herein, we have rationally designed a novel inorganic binder, ammonium polyphosphate (APP), which combines several attractive properties for high performance Li−S batteries including (1) moderate binding strength to maintain integrity of the electrode material; (2) strong affinity with LiPSs via chemical interaction to suppress the dissolution of LiPSs as the main chain of the inorganic polymer binder can be highly polarized chemical bonds, which can bind LiPSs more efficiently (the carbon−carbon bonds in the main chain of conventional organic polymer binders cannot bind LiPSs efficiently); (3) flame-retardant property to improve safety, a property conventional organic polymer binders do not have; (4) facilitation of Li ion transport to accelerate redox chemistry and promote the reaction kinetics; and (5) water solubility for environmentally friendly processing.

RESULTS AND DISCUSSION

APP is commercially used as a food additive, emulsifier, and fertilizer available at large scale and low cost (Figure 1a). Here we employ it as a multifunctional binder. The absorptivity of APP and commonly used PVDF binder toward LiPSs was quantitatively evaluated by adding different masses of binder with the same total surface area (calculated based on the BET specific surface area) into a dioxolane/dimethoxyethane (DOL/DME, 1:1, v:v) solution containing 0.005 M Li_2S_6. After adsorption and rest for 4 h, there is no obvious color change of the polysulfide solution after adsorption by PVDF, suggesting weak adsorption of polysulfide (Figure 1b). In sharp contrast, APP demonstrates significant polysulfide adsorption capability and the color of the polysulfide solution changes from yellow to nearly colorless, indicating strong interaction between Li_2S_6 and APP binder. In order to further probe the polysulfide trapping ability of different binders, the supernatant liquid of the three bottles after adsorption was analyzed by ultraviolet−visible (UV−vis) absorption spectroscopy, and the concentration variation of Li_2S_6 solution before and after adding various binders is shown in Figure 1c. All samples exhibited a broad absorption region between 250 and 350 nm, and the characteristic peaks located around 260, 280, 300, and 340 nm can be attributed to S_6^{2-} species.[35−37] Compared with pristine Li_2S_6 solution, the peak intensities of the solution soaked with PVDF decreased slightly, while the absorption peak intensities of the APP solution decreased much more sharply. The APP binder adsorbs roughly twice as much polysulfide as the PVDF binder, as indicated by the much lower concentration of Li_2S_6 remaining in the solution and demonstrating the strong affinity of the S_6^{2-} species to the APP binder.

In order to clarify the enhancement of binding strength by inorganic APP polymer, first-principles simulations were carried out on the adsorption of Li−S species on APP and PVDF. The binding energies between the LiPS species and two polymers

DOI: 10.1021/acscentsci.7b00569
ACS Cent. Sci. 2018, 4, 260−267

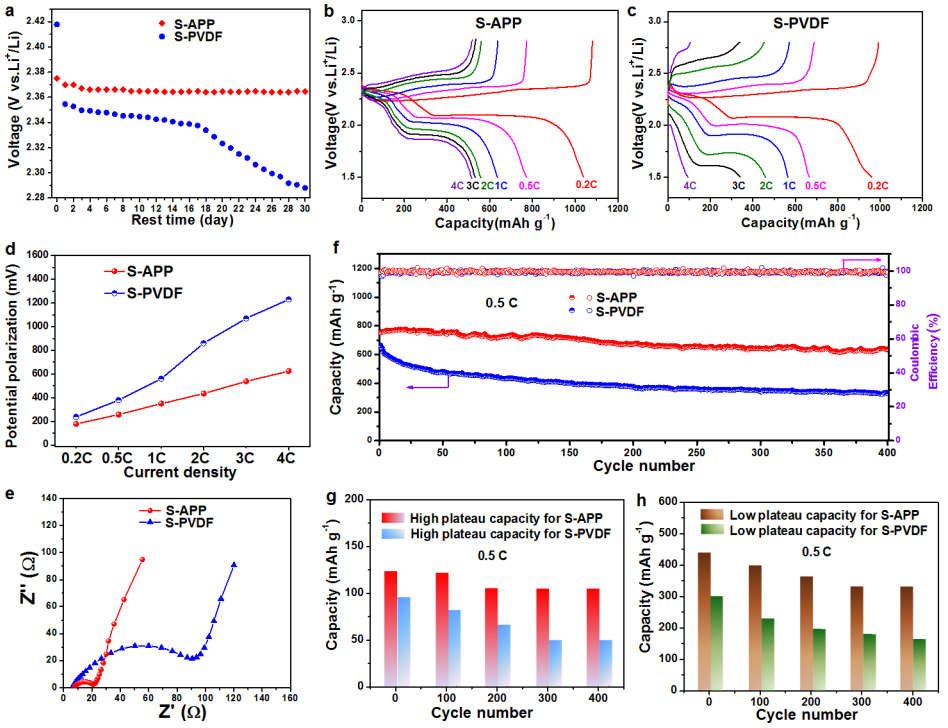

Figure 2. Electrochemical performance. (a) Self-discharge behavior of Li−S batteries with APP and PVDF binders. Charge/discharge voltage profiles of the (b) S-APP and (c) S-PVDF electrodes at various rates. (d) Comparison of the potential polarization between the charge and discharge plateaus at different current densities. (e) Nyquist plots of the S-APP and S-PVDF electrodes at open circuit before cycling at room temperature. (f) Long-term cycling stability and Coulombic efficiency of the S-APP and S-PVDF electrodes at 0.5 C for 400 cycles after the rate capability test. (g) High plateau and (h) low plateau capacity for S-APP and S-PVDF electrodes obtained from panel f.

are computed to evaluate the interaction strength between them, which can be expressed as $E_b = E_P + E_{LiS} - E_{P\text{-}LiS}$ ($E_{P\text{-}LiS}$, E_P, and E_{LiS} are the total energies for the adsorption system, isolated polymer, and isolated Li−S species respectively). A larger E_b indicates stronger interaction. The van der Waals force is also included in the computation, which we have shown to be crucial for the cathode material system of Li−S battery.[38] The Li−S species we chose for simulation are Li_2S, Li_2S_2, Li_2S_4, Li_2S_6, and Li_2S_8, which can cover the whole lithiation process and represent all of the typical species in the fully lithiated, middle-lithiated, and under-lithiated stages. The chemical structures as well as adsorption conformations are illustrated in Figure 1d−g and Figure S1. The binding strengths of various LiPS species on two kinds of polymer binders are demonstrated in Figure 1h and Table S1. It can be clearly seen that APP polymer can induce binding energies in the region of 2.16−2.30 eV, much higher than those of PVDF (0.58−0.74 eV). Such interaction strength is also much stronger compared with other common organic polymer binders, such as PVP, PEDOT, polyaniline, and so on,[34,39] and even comparable with metal sulfides in our previous study.[21]

According to the adsorption conformations, chemical bonds are formed between the positively charged Li^+ in the Li−S species and the negatively charged O^{2-} (in APP) or F^- (in PVDF). It is expected that the distinction in binding strength can be attributed to different bonds inside the polymers: the P−O bond in APP and the C−F bond in PVDF. Here, to clarify the difference between binding strengths, the Bader charge analysis is applied[40,41] to evaluate the real valence charge state for various atoms and the number of electrons that transfer between them. In Table S2, the Bader charge variances on the key atoms (P and O atoms in APP, C and F atoms in PVDF) are listed. It can be seen that the O atom in APP gains the largest number of electrons, while the P atom loses the largest number accordingly, which means that the largest localized polarization strength can be induced in the P−O chain, and as a result, strong binding interaction can be formed. In contrast, the lowest amount of electron transfer occurs on the C−F bond in PVDF and therefore the smallest polarization strength results in the weakest interaction strength. Strong charge transfer and strong polarization inside the P−O chain can be mainly attributed to the different properties of elemental P and C. According to atomic electronegativity, P atom can lose a valence electron much more easily than a C atom, and as a result, the P-based inorganic polymer possesses obvious advantage over the C-based organic polymer. Furthermore, Li−S species can concentrate on the P−O main-body chain, which is different from the organic polymer case, in which the Li−S species are mainly attached to the side chain.[34]

Important requirements for binders include good swelling in the electrolyte to maintain electrolyte immersion and high viscosity to enable good mechanical properties of the electrode. To determine the electrolyte uptake ability of the two binders, the swelling ratios of APP and PVDF are tested at different times and shown in Figure 1i. Sodium carboxymethyl cellulose (CMC) and poly(acrylic acid) (PAA) are selected as aqueous binders for comparison, and the corresponding swelling property is shown in Figure S2. APP binder exhibits an electrolyte uptake of around 40% after 10 min, much higher than the uptake of CMC, PVDF, and PAA binders with limited values of ∼28%, 20%, and 4% measured after 30 min. APP binder's higher uptake suggests that it can effectively adsorb and maintain electrolyte in the electrode structure to improve ion accessibility and reaction kinetics. The viscosity of 5 wt %

DOI: 10.1021/acscentsci.7b00569
ACS Cent. Sci. 2018, 4, 260−267

solutions of APP and PVDF binders was measured (Figure S3) to demonstrate the mechanical binding strength of each polymer. The viscosity of APP binder solution is similar to the commonly used PVDF solution, suggesting that its moderate bonding strength is capable of sustaining the structural stability of electrode materials during discharge/charge processes. The adhesion strength of the S-APP electrode material to the current collector is also measured and demonstrates sufficient binding to adhere the active materials together (Figure S4).

Severe self-discharge behavior, caused by the shuttle effect, is one of the main drawbacks of Li−S batteries leading to voltage drop and capacity decay.[42] The variation of the open circuit voltage (OCV) during rest was monitored to show the self-discharge of sulfur cathodes with different binders (Figure 2a). It was observed that the OCV of the S-PVDF electrode drops drastically from 2.42 to 2.29 V after 30 days, indicating the transformation from sulfur and high order polysulfide to low order polysulfide during the self-discharge process.[43] In sharp contrast, the S-APP electrode shows almost no voltage drop during the 30 day rest, demonstrating that self-discharge was significantly inhibited. This can be explained by the reduction in dissolution and diffusion of sulfur/high-order polysulfides through the strong binding of the main chain of APP. Figures 2b and 2c show the galvanostatic charge/discharge profiles of S-APP and S-PVDF electrodes within the voltage window of 1.5−2.8 V vs Li^+/Li^0. The S-APP electrode exhibited typical two-plateau discharge curves from 0.2 C to a high rate of 4 C, which corresponds to the reduction of elemental sulfur (S_8) to long-chain LiPSs (Li_2S_x, $4 \leq x \leq 8$) at high voltages and the formation of short-chain Li_2S_2/Li_2S at lower voltages.[44,45] When scanning in the reverse direction, there are two oxidation plateaus representing the transformation of Li_2S/Li_2S_2 to long-chain Li_2S_x and sulfur. All the plateaus are flat and stable with low polarization, suggesting a kinetically efficient reaction process with a small barrier.[45,46] However, the overpotential grows larger when the current density is increased and the charge/discharge plateaus obviously shift or even disappear at high current rates for S-PVDF electrode, which indicate high polarization and slow redox reaction kinetics with low S utilization (Figures 2c and 2d). A highly reversible average capacity of 1035 mAh g^{-1} is obtained at 0.2 C, and 520 mAh g^{-1} is still achieved when the C-rate was increased to as high as 4 C, indicating fast reaction kinetics in the S-APP electrode. These capacities are much higher than those for the sulfur cathode with PVDF binder tested under the same conditions (Figures 2b and 2c).

Electrochemical impedance spectroscopy (EIS) measurements were performed to determine the Li ion conductivity of cells with APP and PVDF binders (Figure 2e). Nyquist plots for the cells demonstrate a suppressed semicircle in the high/medium frequency regions followed by an inclined line in the low frequency region, which corresponds to the charge transfer resistance (R_{ct}) and a mass-transfer process.[47] The lower R_{ct} of S-APP cathode compared to S-PVDF cathode indicates that APP helps to reduce the charge transfer resistance and thus contributes to the reduction in polarization. It was also observed that the slope of the inclined line in the low frequency region for the APP binder-based sulfur electrode is larger than for the S-PVDF electrode, implying favorable Li ion transfer, which is in agreement with the charge/discharge profiles. A schematic diagram is depicted in Figure S5 to represent the mechanism of the improved Li ion transportation enabled by APP binder. The positively charged lithium ion may be coupled with the negatively charged side chain of APP, facilitating fast Li^+ transport.

Long-term cycling stability of different sulfur electrodes was tested at a C-rate of 0.5 C for 400 cycles. The S-APP electrode exhibits an initial reversible capacity of 753 mAh g^{-1}, and the capacity remains at 640 mAh g^{-1} after 400 cycles with a Coulombic efficiency above 99% during cycling, corresponding to a capacity retention of 85.0% and capacity decay of only 0.038% per cycle (Figure 2f). However, the capacity of S-PVDF electrode rapidly decreases to 329 mAh g^{-1} after 400 cycles with a capacity retention of 49.6%, and capacity decay rate as high as 0.126% per cycle, suggesting that the weak affinity of PVDF with LiPSs cannot hinder their dissolution into the electrolyte. The high plateau and low plateau capacity contributions to the total discharge capacity for S-APP and S-PVDF electrodes were further analyzed (Figures 2g and 2h). The capacity of S-APP electrode, whether at high plateau or low plateau, is much higher and more stable compared to S-PVDF electrode, confirming the suppression of polysulfide dissolution by APP. To further improve the energy density of Li−S batteries, the active material loading of the electrode is increased to 5.6 mg cm^{-2} and the S-APP electrode still exhibits good cycling performance with reversible discharge capacities reaching 530 mAh g^{-1} at 0.5 C rate after 200 cycles (Figure S6). However, the S-PVDF cathode decays quickly with a capacity of only 320 mAh g^{-1} after 200 cycles, demonstrating its inferior cycling performance. These results demonstrate that batteries with APP binder exhibit higher sulfur utilization and better capacity retention upon cycling compared to the conventional PVDF binder. The remarkably improved performance indicates that APP binder is effective in confining polysulfides/Li_2S within the cathode and inhibiting polysulfide shuttling through strong chemical binding, thereby extending the cycling life of Li−S batteries. The facilitated ion transport during the redox of sulfur is responsible for the excellent rate behavior and decreased polarization of the electrode.

The safety concerns surrounding Li−S batteries originating from the flammability of lithium, sulfur electrodes, and liquid electrolytes can be alleviated by engineering of the battery structure, employing solid-state electrolyte, and optimizing electrode design.[48−50] The APP binder employed here not only improves the polysulfide adsorption capability but also endows sulfur electrode with flame-retardant properties to effectively improve the safety of Li−S batteries. To demonstrate the flame-retardant property of APP, sulfur cathodes with APP and PVDF binders were exposed to a direct flame until they were ignited, after which the direct flame was removed. Sulfur cathode with traditional PVDF binder was tested using this method as shown in Figure 3a. Upon exposure to direct flame for ∼1 s, the sulfur cathode was ignited and the flame burned vigorously and spread quickly. The specific burning time, i.e., the burning time divided by the mass of sulfur, was calculated to be ∼519 s g^{-1}, reflecting the high flammability of sulfur cathode (Figure 3c). The sulfur cathode with APP binder was tested using the same method. In contrast, APP binder is efficient in reducing the burning time of the sulfur cathode. After being ignited, the flame was suppressed and finally self-extinguished (Figure 3b,c). The specific burning time was significantly decreased to ∼289 s g^{-1}, indicating the flame-retardant properties of the APP binder based sulfur cathode. The flame-retardant mechanism of the APP binder can be supposed as follows: During the combustion process, APP decomposes and releases

DOI: 10.1021/acscentsci.7b00569
ACS Cent. Sci. 2018, 4, 260−267

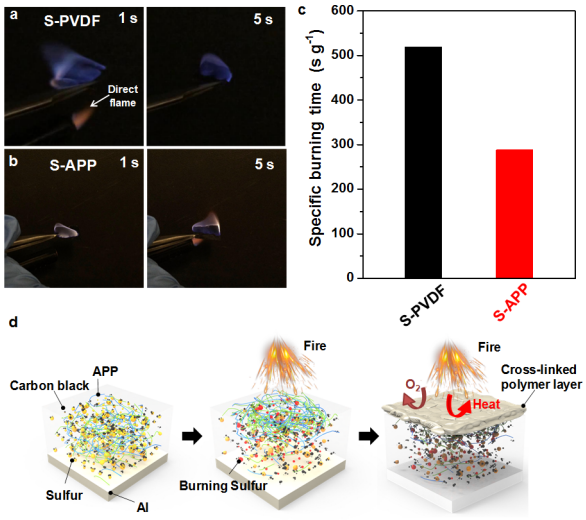

Figure 3. Flame-retardant properties. The specific burning time test of sulfur electrodes with (a) S-PVDF electrode and (b) S-APP electrode. The times indicated in the pictures are counted as soon as the electrodes are exposed to the direct flame from a lighter (indicated by the white arrow in panel a). (c) The specific burning time of the sulfur cathodes with APP and PVDF binders. (d) Schematic showing the flame-retardant mechanism of the APP binder based sulfur electrode.

ammonia/water gas, and cross-links to form an insulating polymer layer (Figure 3d and Figure 4a). This insulating polymer layer acts as a physical barrier to heat, fuel, and oxygen transfer, thus building up an isolation layer between the condensed and gas phases and effectively protecting the underlying sulfur from catching fire (Figure 3d).

To confirm the proposed flame-retardant mechanism, we did a burning test on S-APP and S-PVDF electrodes and, after the fire was self-extinguished, X-ray photoelectron spectroscopy (XPS) and scanning electron microscopy (SEM) were used to understand the mechanism. XPS analysis clearly shows the presence of nitrogen, sulfur, and phosphorus elements in the S-APP electrode from the survey spectrum (Figure 4b). After burning, the intensity of the N 1s signal significantly decreases, while the intensity of the phosphorus signal is almost the same, indicating decomposition and release of NH_3, as well as generating a cross-linked polymer, as proposed in Figure 4a. It should be noted that the sulfur signal only slightly decreases, suggesting that the APP binder protects the underlying sulfur from burning and halts the further spread of the fire. This is quite different for the S-PVDF electrode based on the S 2p XPS spectrum analysis, in which the intensity of the sulfur signal obviously decreases, suggesting that most of the sulfur materials are burned away (Figure 4c). X-ray diffraction (XRD) measurements were also carried out for APP and its ignition products as shown in Figure S7. Many strong APP crystal peaks appear between 5 and 55 degrees, whereas all of the peaks disappear after ignition, suggesting its formation into an amorphous cross-linked polymer. This is evidence for the existence of a protective layer after ignition of APP and is consistent with the XPS analysis. Further evidence can be obtained from the SEM post-mortem analysis of the electrodes after burning. The overall morphology and structure were well preserved for S-APP electrode (Figure 4d and Figure S8a,b), demonstrating that the protective layer produced by APP decomposition helps prevent further combustion of sulfur. However, due to the weak protection offered by PVDF binder, a large quantity of sulfur is evaporated from the sulfur cathode, leaving many holes in the electrode after burning (Figure 4h and Figure S8c,d) which is in agreement with the previous analysis. The corresponding sulfur and phosphorus elemental maps of the S-APP electrode after burning indicate that sulfur is

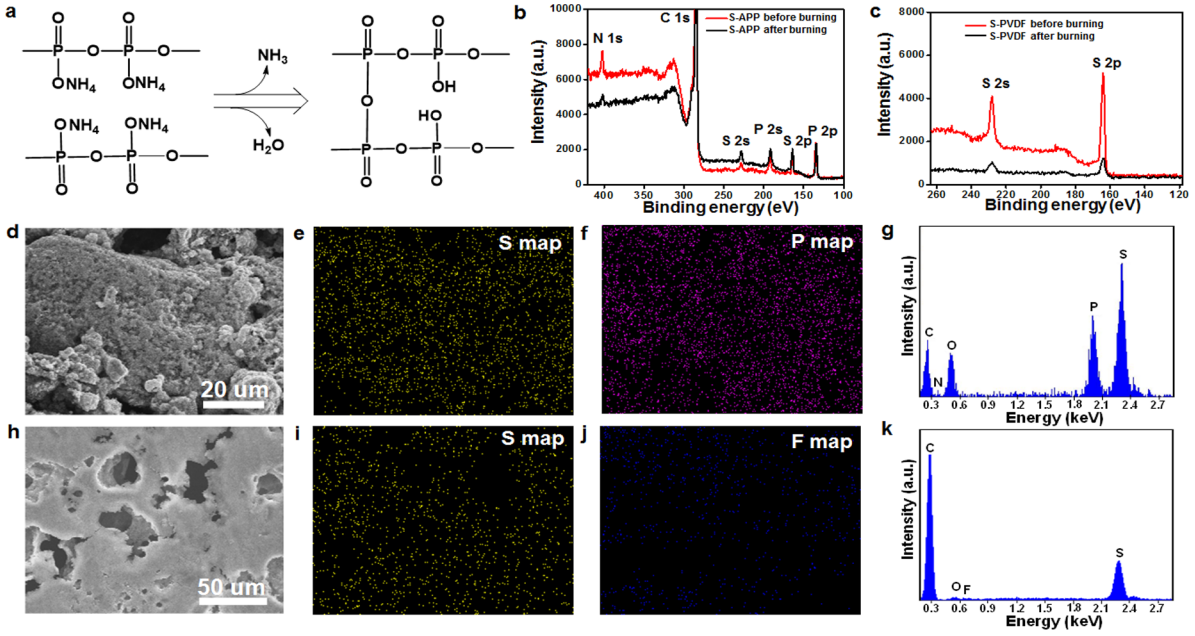

Figure 4. Flame-retardant mechanism and post-mortem analysis of the electrodes after burning. (a) Chemical reaction for flame-retardant mechanism. (b) XPS spectra of the surface chemical composition of the S-APP electrode before and after burning. (c) S 2p XPS spectra of the S-PVDF electrode before and after burning. (d) SEM image and the corresponding (e) sulfur and (f) phosphorus elemental maps of the S-APP electrode after burning. (g) EDS of the S-APP electrode after burning. (h) SEM image and the corresponding (i) sulfur and (j) fluorine elemental maps of the S-PVDF electrode after burning. (k) EDS of the S-PVDF electrode after burning.

DOI: 10.1021/acscentsci.7b00569
ACS Cent. Sci. 2018, 4, 260−267

protected and phosphorus is retained in the electrode (Figure 4e,f), which is consistent with the EDS results that the intensity of the sulfur signal is much higher compared with the carbon signal from the electrode (Figure 4g). In contrast, holes are found on the sulfur cathode with PVDF binder (Figure 4h,j), and the sulfur signal is missing in these areas (Figure 4i), indicating poor protection of sulfur combustion by PVDF. In addition, the sulfur signal is much lower than the carbon signal after burning (Figure 4k), confirming the evaporation of sulfur from sulfur cathode during the burning process.

SUMMARY

In summary, an aqueous inorganic polymer has been developed as a novel multifunctional binder for high performance Li−S batteries. This aqueous binder, APP, enables a green fabrication procedure which does not employ toxic organic solvents such as NMP. APP performs as a strong polysulfide-trapping agent which blocks the out-diffusion of polysulfide anions and suppresses the shuttling effect, meanwhile promoting the hopping of Li^+ on the APP which is favorable for ion transfer with improved cathode reaction kinetics. Moreover, APP bestows the sulfur cathode with significantly improved flame-retardant property, thus improving the safety of Li−S batteries. Based on this multifunctional binder, the resulting S-APP cathode delivers significantly improved battery performance with high initial specific capacity, good rate performance, and excellent cycling stability for 400 cycles with ∼0.038% capacity decay per cycle. The findings of this work shed light on the design of multifunctional binders for building high-performance Li−S batteries.

EXPERIMENTAL SECTION

Preparation of Binders and Sulfur Cathodes. APP (M_w = 2400) and PVDF (M_w = 455,000) were purchased and used directly. APP was dissolved in deionized water and magnetically stirred to obtain the APP binder. The sulfur electrode was prepared by mixing sulfur powder (60 wt %), carbon black (20 wt %), and APP or PVDF binders (20 wt %).

Adsorption of Lithium Polysulfide. The binders were dried under vacuum at 60 °C overnight before the adsorption test. Li_2S_6 was prepared by chemically reacting sublimed sulfur and an appropriate amount of Li_2S in DOL/DME solution (1:1 by volume). The solution was then stirred at 70 °C in an Ar-filled glovebox overnight to produce a brownish-red Li_2S_6 catholyte solution (1.0 M). The Li_2S_6 solution was then diluted to 0.005 M for the polysulfide adsorption test.

Flame-Retardant Properties. The specific burning time was used to quantitatively estimate the flame-retardant properties of the binders. It was obtained by igniting preweighed sulfur electrodes with APP and PVDF binders. The sulfur electrodes were exposed to a direct flame from a lighter. After the sulfur was ignited, the lighter was removed. Then the time for the flame to self-extinguish was recorded and normalized by the sulfur electrode mass with the same area, obtaining the specific burning time of the sulfur electrodes with various binders.

Adhesion Force Test. Adhesion experiments were performed on an Instron 5565 testing station with a 100 N load cell. Samples approximately 4 cm long by 1 cm wide were cut from calendared electrode sheets. Scotch Magic tape was affixed to the surface and was peeled off at a rate of 500 mm/min as the force was monitored. Three samples were measured for each binding condition.

Materials Characterization. The morphology and microstructure of the samples was investigated by an FEI XL30 Sirion SEM operated at an accelerating voltage of 5 kV. UV−visible absorption spectra were collected with an Agilent Cary 6000i UV−visible−NIR spectrometer with baseline correction. XRD was performed on a PANalyticalX'Pert with Ni-filtered Cu Kα radiation. The specific surface area was tested by nitrogen adsorption−desorption measurement at 77 K (Micromeritics, ASAP 2020). Binder viscosity was measured by TA Instruments ARES-G2 rotational rheometer.

Electrochemical Measurements. Electrochemical experiments were performed using CR2032 coin cells assembled in an argon-filled glovebox with lithium metal as the counter and reference electrodes. Sulfur was ground and mixed with conductive carbon black and either PVDF binder in *N*-methyl-2-pyrrolidinone or APP binder in water (60:20:20 by weight) to form a slurry that was coated onto carbon-coated aluminum foil. The electrode was dried at 60 °C under vacuum for 12 h. The high mass loading of the sulfur electrodes was 5.6 mg cm^{-2}, and the other cases were 2−3 mg cm^{-2}. The corresponding specific capacities were calculated based on the mass of sulfur in the cathodes. Electrolyte was prepared by dissolving an appropriate amount of lithium bis-(trifluoromethanesulfonyl)imide (LiTFSI) (1 M) in 1:1 v/v DME and DOL containing $LiNO_3$ (0.1 M). 20 μL of the electrolyte was added to wet the sulfur cathode. A Celgard 2400 separator was then placed over the electrode, and an additional 20 μL of blank electrolyte was added to the cell. The lithium−metal foil anode was placed on top of the separator. Galvanostatic charge−discharge cycles were performed on a CT2001A cell test instrument (LAND Electronic Co.). The sulfur cathode based cells were measured with the potential range of 1.5−2.8 V (vs Li/Li^+). The C-rate for tests was referred to the mass of sulfur in the cathode and was varied from 0.2 C to 4 C rate. Electrochemical impedance spectroscopy (EIS) data was obtained with a VMP3 potentiostat (Biologic) from 200 kHz to 100 mHz with an ac voltage amplitude of 10 mV at the open-circuit potential.

Simulation Methods. First-principles simulations were applied using the Vienna Ab initio Simulation Package (VASP) in the framework of density functional theory.[51−53] The projector augmented-wave pseudopotential was used while the generalized gradient approximation exchange-correlation function was described by Perdew−Burke−Ernzerhof scheme.[54] The plane-wave basis is adopted, and 600 eV was chosen as the cutoff energy to ensure the precision of calculations. The vacuum between polymer and its image is larger than 20 Å, while the distance between Li−S species and its image is no less than 15 Å along the periodic direction. These systems are large enough to avoid artificial interaction caused by periodicity. The vdW-DF2 functional is added in computation,[55,56] in order to include the van der Waals interaction. The 3D atomic visualization models were plotted using VESTA-3.0 software.[57]

ASSOCIATED CONTENT

Supporting Information

The Supporting Information is available free of charge on the ACS Publications website at DOI: 10.1021/acscentsci.7b00569.

DOI: 10.1021/acscentsci.7b00569
ACS Cent. Sci. 2018, 4, 260−267

Additional characterizations including adsorption conformations, binding strengths, swelling ratios, viscosity, high mass loading performance, XRD patterns, and SEM images of electrodes before and after ignition (PDF)

AUTHOR INFORMATION

Corresponding Authors

*E-mail: qianfan@buaa.edu.cn.
*E-mail: yicui@stanford.edu.

ORCID

Guangmin Zhou: 0000-0002-3629-5686
Kai Liu: 0000-0003-3362-180X
Wei Liu: 0000-0002-6206-8321
Feifei Shi: 0000-0002-9171-6180
Wei Chen: 0000-0001-7701-1363
Jeffrey Lopez: 0000-0002-6425-5550
Jie Zhao: 0000-0001-6446-8313
Yi Cui: 0000-0002-6103-6352

Author Contributions

‡G.Z., K.L., and Y.F. contributed equally to this work.

Notes

The authors declare no competing financial interest.

ACKNOWLEDGMENTS

This work was supported by the Assistant Secretary for Energy Efficiency and Renewable Energy, Office of Vehicle Technologies of the U.S. Department of Energy, under the Battery Materials Research program and the Battery 500 Consortium program. Q.Z. is supported by the National Natural Science Foundation of China (11404017), the Technology Foundation for Selected Overseas Chinese Scholar, the Ministry of Human Resources and Social Security of China, and the program for New Century Excellent Talents in University (NCET-12-0033).

REFERENCES

(1) Bruce, P. G.; Freunberger, S. A.; Hardwick, L. J.; Tarascon, J.-M. Li-O_2 and Li-S batteries with high energy storage. *Nat. Mater.* **2012**, *11*, 19−29.
(2) Yang, Y.; Zheng, G.; Cui, Y. Nanostructured sulfur cathodes. *Chem. Soc. Rev.* **2013**, *42*, 3018−3032.
(3) Sun, Y.; Liu, N.; Cui, Y. Promises and challenges of nanomaterials for lithium-based rechargeable batteries. *Nat. Energy* **2016**, *1*, 16071.
(4) Manthiram, A.; Fu, Y.; Chung, S.-H.; Zu, C.; Su, Y.-S. Rechargeable Lithium−Sulfur Batteries. *Chem. Rev.* **2014**, *114*, 11751−11787.
(5) Wang, D.-W.; Zeng, Q.; Zhou, G. M.; Yin, L.; Li, F.; Cheng, H.-M.; Gentle, I. R.; Lu, G. Q. M. Carbon-sulfur composites for Li-S batteries: status and prospects. *J. Mater. Chem. A* **2013**, *1*, 9382−9394.
(6) Chung, W. J.; Griebel, J. J.; Kim, E. T.; Yoon, H.; Simmonds, A. G.; Ji, H. J.; Dirlam, P. T.; Glass, R. S.; Wie, J. J.; Nguyen, N. A.; Guralnick, B. W.; Park, J.; Somogyi, Á.; Theato, P.; Mackay, M. E.; Sung, Y.-E.; Char, K.; Pyun, J. The use of elemental sulfur as an alternative feedstock for polymeric materials. *Nat. Chem.* **2013**, *5*, 518−524.
(7) Choi, J. W.; Aurbach, D. Promise and reality of post-lithium-ion batteries with high energy densities. *Nat. Rev. Mater.* **2016**, *1*, 16013.
(8) Pang, Q.; Liang, X.; Kwok, C. Y.; Nazar, L. F. Advances in lithium−sulfur batteries based on multifunctional cathodes and electrolytes. *Nat. Energy* **2016**, *1*, 16132.
(9) Jin, Y.; Zhou, G.; Shi, F.; Zhuo, D.; Zhao, J.; Liu, K.; Liu, Y.; Zu, C.; Chen, W.; Zhang, R.; Huang, X.; Cui, Y. Reactivation of dead sulfide species in lithium polysulfide flow battery for grid scale energy storage. *Nat. Commun.* **2017**, *8*, 462.
(10) Ji, X. L.; Lee, K. T.; Nazar, L. F. A highly ordered nanostructured carbon-sulphur cathode for lithium-sulphur batteries. *Nat. Mater.* **2009**, *8*, 500−506.
(11) Zheng, G.; Zhang, Q.; Cha, J. J.; Yang, Y.; Li, W.; Seh, Z. W.; Cui, Y. Amphiphilic Surface Modification of Hollow Carbon Nanofibers for Improved Cycle Life of Lithium Sulfur Batteries. *Nano Lett.* **2013**, *13*, 1265−1270.
(12) Jayaprakash, N.; Shen, J.; Moganty, S. S.; Corona, A.; Archer, L. A. Porous Hollow Carbon@Sulfur Composites for High-Power Lithium-Sulfur Batteries. *Angew. Chem., Int. Ed.* **2011**, *50*, 5904−5908.
(13) Li, L.; Wu, Z. P.; Sun, H.; Chen, D.; Gao, J.; Suresh, S.; Chow, P.; Singh, C. V.; Koratkar, N. A Foldable Lithium−Sulfur Battery. *ACS Nano* **2015**, *9*, 11342−11350.
(14) Xin, S.; Gu, L.; Zhao, N.-H.; Yin, Y.-X.; Zhou, L.-J.; Guo, Y.-G.; Wan, L.-J. Smaller Sulfur Molecules Promise Better Lithium−Sulfur Batteries. *J. Am. Chem. Soc.* **2012**, *134*, 18510−18513.
(15) Zhao, J.; Zhou, G.; Yan, K.; Xie, J.; Li, Y.; Liao, L.; Jin, Y.; Liu, K.; Hsu, P.-C.; Wang, J.; Cheng, H.-M.; Cui, Y. Air-stable and freestanding lithium alloy/graphene foil as an alternative to lithium metal anodes. *Nat. Nanotechnol.* **2017**, *12*, 993.
(16) Zhou, G.; Sun, J.; Jin, Y.; Chen, W.; Zu, C.; Zhang, R.; Qiu, Y.; Zhao, J.; Zhuo, D.; Liu, Y.; Tao, X.; Liu, W.; Yan, K.; Lee, H. R.; Cui, Y. Sulfiphilic Nickel Phosphosulfide Enabled Li_2S Impregnation in 3D Graphene Cages for Li−S Batteries. *Adv. Mater.* **2017**, *29*, 1603366.
(17) Peng, H.-J.; Hou, T.-Z.; Zhang, Q.; Huang, J.-Q.; Cheng, X.-B.; Guo, M.-Q.; Yuan, Z.; He, L.-Y.; Wei, F. Strongly Coupled Interfaces between a Heterogeneous Carbon Host and a Sulfur-Containing Guest for Highly Stable Lithium-Sulfur Batteries: Mechanistic Insight into Capacity Degradation. *Adv. Mater. Interfaces* **2014**, *1*, 1400227.
(18) Wang, Z.; Dong, Y.; Li, H.; Zhao, Z.; Bin Wu, H.; Hao, C.; Liu, S.; Qiu, J.; Lou, X. W. Enhancing lithium−sulphur battery performance by strongly binding the discharge products on amino-functionalized reduced graphene oxide. *Nat. Commun.* **2014**, *5*, 5002.
(19) Tao, X.; Wang, J.; Liu, C.; Wang, H.; Yao, H.; Zheng, G.; Seh, Z. W.; Cai, Q.; Li, W.; Zhou, G.; Zu, C.; Cui, Y. Balancing surface adsorption and diffusion of lithium-polysulfides on nonconductive oxides for lithium-sulfur battery design. *Nat. Commun.* **2016**, *7*, 11203.
(20) Pang, Q.; Kundu, D.; Cuisinier, M.; Nazar, L. F. Surface-enhanced redox chemistry of polysulphides on a metallic and polar host for lithium-sulphur batteries. *Nat. Commun.* **2014**, *5*, 4759.
(21) Seh, Z. W.; Yu, J. H.; Li, W.; Hsu, P.-C.; Wang, H.; Sun, Y.; Yao, H.; Zhang, Q.; Cui, Y. Two-dimensional layered transition metal disulphides for effective encapsulation of high-capacity lithium sulphide cathodes. *Nat. Commun.* **2014**, *5*, 5017.
(22) Pang, Q.; Kundu, D.; Nazar, L. F. A graphene-like metallic cathode host for long-life and high-loading lithium-sulfur batteries. *Mater. Horiz.* **2016**, *3*, 130−136.
(23) Demir-Cakan, R.; Morcrette, M.; Nouar, F.; Davoisne, C.; Devic, T.; Gonbeau, D.; Dominko, R.; Serre, C.; Ferey, G.; Tarascon, J. M. Cathode composites for Li-S batteries via the use of oxygenated porous architectures. *J. Am. Chem. Soc.* **2011**, *133*, 16154−16160.
(24) Wang, J. L.; Yang, J.; Xie, J. Y.; Xu, N. X. A novel conductive polymer-sulfur composite cathode material for rechargeable lithium batteries. *Adv. Mater.* **2002**, *14*, 963−965.
(25) Wang, L.; He, X.; Li, J.; Chen, M.; Gao, J.; Jiang, C. Charge/discharge characteristics of sulfurized polyacrylonitrile composite with different sulfur content in carbonate based electrolyte for lithium batteries. *Electrochim. Acta* **2012**, *72*, 114−119.
(26) Xiao, L. F.; Cao, Y. L.; Xiao, J.; Schwenzer, B.; Engelhard, M. H.; Saraf, L. V.; Nie, Z. M.; Exarhos, G. J.; Liu, J. A Soft Approach to Encapsulate Sulfur: Polyaniline Nanotubes for Lithium-Sulfur Batteries with Long Cycle Life. *Adv. Mater.* **2012**, *24*, 1176−1181.
(27) Li, W.; Zheng, G.; Yang, Y.; Seh, Z. W.; Liu, N.; Cui, Y. High-performance hollow sulfur nanostructured battery cathode through a scalable, room temperature, one-step, bottom-up approach. *Proc. Natl. Acad. Sci. U. S. A.* **2013**, *110*, 7148−7153.

DOI: 10.1021/acscentsci.7b00569
ACS Cent. Sci. 2018, 4, 260−267

(28) Su, Y.-S.; Manthiram, A. Lithium−sulphur batteries with a microporous carbon paper as a bifunctional interlayer. *Nat. Commun.* **2012**, *3*, 1166.
(29) Huang, J.-Q.; Zhang, Q.; Wei, F. Multi-functional separator/interlayer system for high-stable lithium-sulfur batteries: Progress and prospects. *Energy Storage Materials* **2015**, *1*, 127−145.
(30) Hong, X.; Jin, J.; Wen, Z.; Zhang, S.; Wang, Q.; Shen, C.; Rui, K. On the dispersion of lithium-sulfur battery cathode materials effected by electrostatic and stereo-chemical factors of binders. *J. Power Sources* **2016**, *324*, 455−461.
(31) Bhattacharya, P.; Nandasiri, M. I.; Lv, D.; Schwarz, A. M.; Darsell, J. T.; Henderson, W. A.; Tomalia, D. A.; Liu, J.; Zhang, J.-G.; Xiao, J. Polyamidoamine dendrimer-based binders for high-loading lithium−sulfur battery cathodes. *Nano Energy* **2016**, *19*, 176−186.
(32) Sun, J.; Huang, Y.; Wang, W.; Yu, Z.; Wang, A.; Yuan, K. Application of gelatin as a binder for the sulfur cathode in lithium−sulfur batteries. *Electrochim. Acta* **2008**, *53*, 7084−7088.
(33) Wang, J.; Yao, Z.; Monroe, C. W.; Yang, J.; Nuli, Y. Carbonyl-β-Cyclodextrin as a Novel Binder for Sulfur Composite Cathodes in Rechargeable Lithium Batteries. *Adv. Funct. Mater.* **2013**, *23*, 1194−1201.
(34) Seh, Z. W.; Zhang, Q.; Li, W.; Zheng, G.; Yao, H.; Cui, Y. Stable cycling of lithium sulfide cathodes through strong affinity with a bifunctional binder. *Chem. Sci.* **2013**, *4*, 3673−3677.
(35) Barchasz, C.; Molton, F.; Duboc, C.; Lepretre, J. C.; Patoux, S.; Alloin, F. Lithium/Sulfur Cell Discharge Mechanism: An Original Approach for Intermediate Species Identification. *Anal. Chem.* **2012**, *84*, 3973−3980.
(36) Han, K.; Shen, J.; Hao, S.; Ye, H.; Wolverton, C.; Kung, M. C.; Kung, H. H. Free-Standing Nitrogen-doped Graphene Paper as Electrodes for High-Performance Lithium/Dissolved Polysulfide Batteries. *ChemSusChem* **2014**, *7*, 2545−2553.
(37) Zhou, G. M.; Zhao, Y.; Zu, C.; Manthiram, A. Free-standing TiO_2 nanowire-embedded graphene hybrid membrane for advanced Li/dissolved polysulfide batteries. *Nano Energy* **2015**, *12*, 240−249.
(38) Zhang, Q.; Wang, Y.; Seh, Z. W.; Fu, Z.; Zhang, R.; Cui, Y. Understanding the Anchoring Effect of Two-Dimensional Layered Materials for Lithium−Sulfur Batteries. *Nano Lett.* **2015**, *15*, 3780−3786.
(39) Li, W.; Zhang, Q.; Zheng, G.; Seh, Z. W.; Yao, H.; Cui, Y. Understanding the Role of Different Conductive Polymers in Improving the Nanostructured Sulfur Cathode Performance. *Nano Lett.* **2013**, *13*, 5534−5540.
(40) Henkelman, G.; Arnaldsson, A.; Jonsson, H. A fast and robust algorithm for Bader decomposition of charge density. *Comput. Mater. Sci.* **2006**, *36*, 354−360.
(41) Tang, W.; Sanville, E.; Henkelman, G. A grid-based Bader analysis algorithm without lattice bias. *J. Phys.: Condens. Matter* **2009**, *21*, 084204.
(42) Huang, J.-Q.; Zhuang, T.-Z.; Zhang, Q.; Peng, H.-J.; Chen, C.-M.; Wei, F. Permselective Graphene Oxide Membrane for Highly Stable and Anti-Self-Discharge Lithium−Sulfur Batteries. *ACS Nano* **2015**, *9*, 3002−3011.
(43) Ai, G.; Dai, Y.; Ye, Y.; Mao, W.; Wang, Z.; Zhao, H.; Chen, Y.; Zhu, J.; Fu, Y.; Battaglia, V.; Guo, J.; Srinivasan, V.; Liu, G. Investigation of surface effects through the application of the functional binders in lithium sulfur batteries. *Nano Energy* **2015**, *16*, 28−37.
(44) Ji, X. L.; Nazar, L. F. Advances in Li-S batteries. *J. Mater. Chem.* **2010**, *20*, 9821−9826.
(45) Zhou, G. M.; Wang, D.-W.; Li, F.; Hou, P.-X.; Yin, L.; Liu, C.; Lu, G. Q.; Gentle, I. R.; Cheng, H.-M. A flexible nanostructured sulphur-carbon nanotube cathode with high rate performance for Li-S batteries. *Energy Environ. Sci.* **2012**, *5*, 8901−8906.
(46) Zheng, G. Y.; Yang, Y.; Cha, J. J.; Hong, S. S.; Cui, Y. Hollow Carbon Nanofiber-Encapsulated Sulfur Cathodes for High Specific Capacity Rechargeable Lithium Batteries. *Nano Lett.* **2011**, *11*, 4462−4467.
(47) Zhou, G. M.; Li, L.; Wang, D.-W.; Shan, X.-y.; Pei, S.; Li, F.; Cheng, H.-M. A Flexible Sulfur-Graphene-Polypropylene Separator Integrated Electrode for Advanced Li−S Batteries. *Adv. Mater.* **2015**, *27*, 641−647.
(48) Liu, Y.; Zhou, G.; Liu, K.; Cui, Y. Design of Complex Nanomaterials for Energy Storage: Past Success and Future Opportunity. *Acc. Chem. Res.* **2017**, *50*, 2895−2905.
(49) Fu, K.; Gong, Y.; Dai, J.; Gong, A.; Han, X.; Yao, Y.; Wang, C.; Wang, Y.; Chen, Y.; Yan, C.; Li, Y.; Wachsman, E. D.; Hu, L. Flexible, solid-state, ion-conducting membrane with 3D garnet nanofiber networks for lithium batteries. *Proc. Natl. Acad. Sci. U. S. A.* **2016**, *113*, 7094−7099.
(50) Li, Y.; Fu, K. K.; Chen, C.; Luo, W.; Gao, T.; Xu, S.; Dai, J.; Pastel, G.; Wang, Y.; Liu, B.; Song, J.; Chen, Y.; Yang, C.; Hu, L. Enabling High-Areal-Capacity Lithium−Sulfur Batteries: Designing Anisotropic and Low-Tortuosity Porous Architectures. *ACS Nano* **2017**, *11*, 4801−4807.
(51) Hohenberg, P.; Kohn, W. Inhomogeneous Electron Gas. *Phys. Rev.* **1964**, *136*, B864−B871.
(52) Kresse, G.; Furthmuller, J. Efficiency of ab-initio total energy calculations for metals and semiconductors using a plane-wave basis set. *Comput. Mater. Sci.* **1996**, *6*, 15−50.
(53) Kresse, G.; Furthmuller, J. Efficient iterative schemes for ab initio total-energy calculations using a plane-wave basis set. *Phys. Rev. B: Condens. Matter Mater. Phys.* **1996**, *54*, 11169−11186.
(54) Perdew, J. P.; Chevary, J. A.; Vosko, S. H.; Jackson, K. A.; Pederson, M. R.; Singh, D. J.; Fiolhais, C. Atoms, molecules, solids, and surfaces: Applications of the generalized gradient approximation for exchange and correlation. *Phys. Rev. B: Condens. Matter Mater. Phys.* **1992**, *46*, 6671−6687.
(55) Klimeš, J.; Bowler, D. R.; Michaelides, A. Chemical accuracy for the van der Waals density functional. *J. Phys.: Condens. Matter* **2010**, *22*, 022201.
(56) Lee, K.; Murray, É. D.; Kong, L.; Lundqvist, B. I.; Langreth, D. C. Higher-accuracy van der Waals density functional. *Phys. Rev. B: Condens. Matter Mater. Phys.* **2010**, *82*, 081101−081104.
(57) Momma, K.; Izumi, F. VESTA: a three-dimensional visualization system for electronic and structural analysis. *J. Appl. Crystallogr.* **2008**, *41*, 653−658.

DOI: 10.1021/acscentsci.7b00569
ACS Cent. Sci. 2018, 4, 260−267